Title

Nanotechnology and machine learning enable circulating tumor cells as a reliable biomarker for radiotherapy responses of gastrointestinal cancer patients.

Authors

Poellmann, Michael
Bu, Jiyoon
Liu, Stanley
et al.

Publication Date

2023-04-15

DOI

10.1016/j.bios.2023.115117

Peer reviewed

HHS Public Access

Author manuscript

Biosens Bioelectron. Author manuscript; available in PMC 2024 April 15.

Published in final edited form as:

Biosens Bioelectron. 2023 April 15; 226: 115117. doi:10.1016/j.bios.2023.115117.

Nanotechnology and Machine Learning Enable Circulating Tumor Cells as a Reliable Biomarker for Radiotherapy Responses of Gastrointestinal Cancer Patients

Michael J. Poellmann[1,2], **Jiyoon Bu**[1,2], **Stanley Liu**[2], **Andrew Z. Wang**[2,3], **Steven N. Seyedin**[4], **Chandrikha Chandrasekharan**[5], **Heejoo Hong**[6], **YoungSoo Kim**[7], **Joseph M. Caster**[8], **Seungpyo Hong**[*,1,2,7,9,10]

[1]Pharmaceutical Sciences Division, University of Wisconsin-Madison, Madison, WI 53705

[2]Capio Biosciences, Inc., Madison, WI and Capio Biosciences Korea, Incheon, KOREA

[3]Department of Radiation Oncology, University of Texas Southwestern Medical Center, Dallas, TX, 75390

[4]Department of Radiation Oncology, University of California Irvine, Irvine, CA, 92697

[5]Department of Internal Medicine, University of Iowa, Iowa City, IA, 52242

[6]Department of Clinical Pharmacology & Therapeutics, Asan Medical Center, University of Ulsan, Seoul, KOREA

[7]Department of Pharmacy, College of Pharmacy, Yonsei University, Incheon 21983, Korea

[8]Department of Radiation Oncology, University of Iowa, Iowa City, IA, 52242

[9]Lachman Institute for Pharmaceutical Development, University of Wisconsin-Madison, Madison, WI 53705

[10]Wisconsin Center for NanoBioSystems, University of Wisconsin-Madison, Madison, WI 53705

Abstract

A highly sensitive, circulating tumor cell (CTC)-based liquid biopsy was used to monitor gastrointestinal cancer patients during treatment to determine if CTC abundance was predictive of disease recurrence. The approach uses a combination of biomimetic cell rolling on recombinant E-selectin and dendrimer-mediated multivalent immunocapture at the nanoscale to purify CTCs from peripheral blood mononuclear cells. Due to the exceptionally high numbers of CTCs captured, a machine learning algorithm approach was developed to efficiently and reliably quantify abundance of immunocytochemically-labeled cells. A convolutional neural network and logistic regression

[*]All correspondence should be addressed to: Prof. Seungpyo Hong, Ph.D., Pharmaceutical Sciences Division, School of Pharmacy, University of Wisconsin-Madison, seungpyo.hong@wisc.edu.

Conflicts of Interest Disclosure

MJP, AZW, and SH are affiliated with Capio Biosciences where SH and AZW have significant equity shares.

model achieved 82.9% true-positive identification of CTCs with a false positive rate below 0.1% on a validation set. The approach was then used to quantify CTC abundance in peripheral blood samples from 27 subjects before, during, and following treatments. Samples drawn from the patients either prior to receiving radiotherapy or early in chemotherapy had a median 50 CTC ml^{-1} whole blood (range 0.6–541.6). We found that the CTC counts drawn 3 months post treatment were predictive of disease progression ($p = 0.045$). This approach to quantifying CTC abundance may be a clinically impactful in the timely determination of gastrointestinal cancer progression or response to treatment.

Keywords

Circulating tumor cell; liquid biopsy; gastrointestinal cancer; convolutional neural network

INTRODUCTION

Current approaches to treatment of gastrointestinal cancer typically involve a combination of chemotherapy and radiation followed by surgery (Palta et al. 2019; Wo et al. 2021). However, even with intensive trimodality therapy, recurrences are common leading to 5-year survival rates ranging from 73–90% for regional or localized colorectal cancer to just 14–42% for regional or localized pancreatic cancer according to 2020 American Cancer Society statistics (ACS 2022). Treatment intensification with adjuvant therapies has been proposed to improve outcomes for patients at the highest risk of recurrence after primary therapy. However, current prognostic methods have undesirable limitations which hinder accurate treatment response assessment and patient stratification. Radiographic (imaging) approaches are expensive, cumbersome to patients, and limited in sensitivity (Nishino 2018). Pathologic biopsy following resectioning also suffers from complications and is limited to the primary tumors that are surgically accessible only. Liquid biopsy, referring to the sampling and analysis of tumor biomarkers from a peripheral blood sample, has emerged as a potential alternative and has demonstrated some promise in gastrointestinal cancer (Lee et al. 2019; Normanno et al. 2018). The only FDA-cleared circulating tumor cell (CTC) enumeration technology, CellSearch (Riethdorf et al. 2018), has been marketed for use with metastatic colorectal cancer (Cohen et al. 2008) since 2007. However, it has not been widely adopted as a tool for treatment monitoring, primarily due to its low sensitivity. Previously reported results using CellSearch are inconsistent, detecting CTCs from 75% or fewer patients with metastatic colorectal cancer (Cayrefourcq et al. 2015; Cohen et al. 2008; Gorges et al. 2016; Heitzer et al. 2013; Iwatsuki et al. 2013; van Dalum et al. 2015), 75% or fewer patients with gastric cancer (Hiraiwa et al. 2008; Iwatsuki et al. 2013; Pernot et al. 2017; Tsai et al. 2016), and less than 50% of patients with pancreatic carcinoma (Bidard et al. 2013; Dotan et al. 2016; Khoja et al. 2012; Okubo et al. 2017). A new liquid biopsy platform that effectively detects blood-circulating biomarkers, such as CTCs, in a clinically significant manner is thus urgently needed.

We have previously described a novel technique that incorporated a nanostructured surface with biomimetic cell rolling for highly sensitive CTC detection and enumeration (Myung et al. 2018b; Myung et al. 2014a; Myung et al. 2011a; Myung et al. 2010; Myung et

al. 2018c). Peripheral blood mononuclear cells (PBMC) were separated from whole blood samples shipped to our laboratory and flowed through a flow chamber containing our engineered capture surface illustrated in Figure 1. Selective capture of CTCs occured by a two-step process. First, recombinant E-selectin selectively recruited leukocytes and CTCs to the capture surface (Hong et al. 2007), inducing biomimetic rolling behavior characteristic of the behavior on inflamed vascular cells (McEver and Zhu 2010). Secondly, poly(amidoamine) (PAMAM) dendrimers promoted multivalent binding of CTCs by conjugated antibodies (Jin et al. 2010; Myung et al. 2014a; Myung et al. 2011a; Myung et al. 2015). The dendrimers enhanced the avidity of antibody binding compared to conjugation with linear polymer tethers (Bu et al. 2020a; Poellmann et al. 2020; Poellmann et al. 2022) and the specific antibodies can be tuned depending on the indication (Bu et al. 2020c). A mixture of antibodies targeting epithelial cell adhesion molecule (EpCAM), epidermal growth factor receptor (EGFR), and human epidermal growth factor receptor 2 (HER2) has previously demonstrated capture rates of 100% with a median 113 CTCs ml^{-1} in primarily head and neck squamous cell carcinoma (HNSCC) patients (Myung et al. 2018b). Captured CTCs were distinguished from nonspecifically-bound white blood cells by immunocytochemistry for nucleated cells positive for pan-cytokeratin (CK) and lacking the leukocyte marker CD45.

While high CTC capture rates resulted in easy-to-read trends over the course of treatments (Myung et al. 2018a), the large numbers necessitated an efficient and consistent approach to enumeration. Manual validation of CTCs is particularly burdensome when CTC numbers reach 100s per sample. Image processing algorithms may be employed to both speed the process and minimize user-to-user variation. Unfortunately, straightforward algorithms that depend on relative signal and morphological parameters to identify CK+/CD45− cells have poor performance due to routine inconsistencies and imperfections typical with fluorescent imaging. Machine learning approaches have been reported for digital imaging and pathology applications in general (Erickson et al. 2017; Madabhushi and Lee 2016) and to identify immunofluorescently-stained CTCs specifically (He et al. 2020; Lannin et al. 2016; Nakamichi et al. 2019; Wang et al. 2021). We therefore developed and trained a convolutional neural network (CNN) (Albawi et al. 2017) for the accurate identification of CTCs on our capture surfaces. Importantly, the CNN can be retrained or updated with true positive CTCs from additional cohorts, continuously improving the accuracy of the approach over time. The development was critical for the efficient and accurate enumeration of CTCs on our surfaces.

In this work, a machine learning approach was developed and validated to identify and quantify immunofluorescently-labelled CTCs captured by biomimetic cell rolling and dendrimer-mediated multivalent binding. The approach was applied to a cohort of patients with gastrointestinal cancer, where we observed relatively high CTC counts in patient samples before receiving chemotherapy and radiation therapy (RT). We further correlated mid-RT and post-RT CTC counts with radiologic response to treatment, pathologic response to treatment, and eventual disease progression. The results suggest that this combination of highly sensitive CTC purification and machine learning-based enumeration may be a valuable tool for the diagnosis of gastrointestinal cancer and for the evaluation of patient response to radiation therapy.

MATERIALS AND METHODS

Materials and dendrimer functionalization

Epoxy-functionalized glass slides were obtained from Tekdon (Myakka City, FL). 5,000 MW, heterobifunctional amine-poly(ethylene glycol)-carboxymethyl polymer (PEG) was obtained from JenKem Technology (Plano, TX), while generation (G7) PAMAM dendrimers were obtained from Dendritech, Inc. (Midland, MI). Succinic anhydride, dimethyl sulfoxide (DMSO), 1-ethyl-3-(3-dimethylaminopropyl)carbodiimide hydrochloride (EDC), N-hydroxysuccinimide (NHS), and 2-[4-(2-hydroxyenthyl)piperazin-1-yl]ethanesulfonic acid (HEPES) were obtained from MilliporeSigma (St. Louis, MO). The capture antibodies aEPCAM (AF960), aHER2 (AF1129), aEGFR (AF231), along with recombinant human E-Selectin/CD62E chimera protein, CF were obtained from R&D Systems (Minneapolis, MN). Vacutainer sodium heparin blood tubes were obtained from BD Biosciences (Franklin Lakes, NJ). Fetal bovine serum (FBS) was obtained from Thermo Fisher Scientific (Waltham, MA), phosphate buffered saline (PBS) from Corning (Corning, NY), Dulbecco's Modified Eagle's Medium from Corning , and Ficoll-Paque Plus from GE Healthcare (Uppsala Sweden). Paraformaldehyde was obtained from Polysciences (Warrington, PA), Triton X-100 from Thermo Fisher Scientific, bovine serum albumin (BSA) from Alfa Aesar (Haverhill, MA). Immunocytochemistry antibodies were anti-wide spectrum cytokeratin (ab9377) from Abcam (Cambridge, United Kingdom), anti-CD45 (555480) from BD Biosciences, and anti-CDX2 from Abcam. The secondary antibodies goat anti-rabbit with Alexa Fluor 647, and goat anti-rabbit with Alexa Fluor 555, and goat anti-mouse with Alexa Fluor 488, and (4',6-Diamidino-2-phenylindole) (DAPI) were from Thermo Fisher Scientific.

Before added to capture surfaces, G7 PAMAM dendrimers were first purified 5 times by centrifugal filtration in DDI water with Amicon 10,000 MWCO centrifugal filters were obtained from EMD Millipore (Burlington, MA), followed by lyophilization for 2 days. The purified dendrimers were then partially carboxylated by reaction with succinic anhydride in dimethyl sulfoxide (DMSO) at a molar ratio of 358:1 between succinic anhydride and dendrimer, resulting in approximately 70% of terminal amines converted to carboxyl groups (Myung et al. 2011a), resulting in a net negative charge and preserving additional amines for EDC/NHS chemistry (Sunoqrot et al. 2013). The partially-carboxylated dendrimers were purified again 5 times using centrifugal filtration in DDI water, lyophilized for 2 days, and resuspended in DDI water to create stock solutions.

CTC capture surface preparation

Capture surfaces were fabricated as previously described (Myung et al. 2018b; Myung et al. 2014a; Myung et al. 2010). Briefly, epoxy-functionalized glass slides were placed in custom-fabricated jigs and treated with 1 ml solution at each step. First, slides were incubated overnight with PEG at 0.5 mg ml^{-1} in DDI water. Each of the PEG-immobilized slides was then activated with 15 mM EDC and 25 mM NHS in 1 ml DDI water for 30 min. The partially carboxylated G7 PAMAM dendrimers at a concentration of 0.1 mg ml^{-1} in HEPES buffer (pH 8) were added to the surface and incubated overnight. The dendrimer-PEG-functionalized surfaces were activated once more with EDC and NHS for

30 min before treatment for 1 h with a mixture of antibodies each at 1 μg ml^{-1} in 1 ml HEPES buffered-saline at pH 8 (Bu et al. 2020b; Myung et al. 2019; Myung et al. 2018a; Myung et al. 2014b; Myung et al. 2011b). Lastly, the antibody-functionalized surfaces were incubated with 1 μg ml^{-1} recombinant human E-selectin in PBS for 1 h. The fully functionalized capture slides were stored at 4°C in PBS for up to four weeks prior to use.

Blood sample collection

Patient recruitment and blood collection was completed at the University of Iowa Hospitals and Clinics according to an IRB-approved protocols (#201802719). Approximately 8–12 mL of blood from each patient was collected in a pair of sodium heparin tubes. The first 2 ml of blood drawn were not collected to avoid collecting skin and other non-blood tissue in the sodium heparin tubes. The collected blood samples were shipped overnight in ambient conditions and were processed 18–48 h after the blood draw. Healthy donor sample collection was completed at University of Wisconsin Health University Hospital according to an IRB-approved protocol (2017–0129), with samples stored at ambient temperature and processed 12–24 h after blood draw.

Blood sample processing

Between 6–12 ml whole blood was mixed 1:1 with PBS containing 2% room-temperature and carefully layered on top of an equivalent volume of Ficoll-Paque Plus. The “buffy coat” consisting of peripheral blood mononuclear cells (PBMC) and CTCs was isolated and rinsed twice using centrifugation with 2% FBS in PBS at 2000 xg for 10 min. Sample processing did not proceed if the buffy coat included a significant amount of coagulated erythrocytes. The final cell pellet was resuspended in 0.1 ml DMEM supplemented with 10% FBS.

The fully functionalized capture slides were placed within custom-fabricated flow chambers consisting of parallel, rectangular flow channels defined by silicone o-rings. Channel dimensions were approximately 55 mm from inlet to outlet, 5 mm wide, and 0.15 mm high (Bu et al. 2020b; Myung et al. 2018a). An injection line (1/16” inner diameter, ~12” long) and a 5 ml syringe (Exelint International, Redondo Beach, CA) was primed with DMEM before pulling the cells into the end. The syringe was placed within a NE-10000 syringe pump (New Era Pump Systems, Farmingdale, NY) and the cells injected into one channel of the flow chamber. The first channel was connected to the second by a short stretch of tubing, and a final stretch of tubing led to a waste container. Cells were injected into a PBS-primed flow chamber for 25 min at a volumetric flow rate of 25 μl min^{-1}, corresponding to 0.36 dyn cm^{-2}, then 15 min at 90 μl min^{-1} (1.3 dyn cm^{-2}) (Bu et al. 2020b; Myung et al. 2018a). The injection line and syringe were replaced with ones containing PBS, and the flow chamber was rinsed in the opposite direction for 15 min at 90 μl min^{-1}. Finally, the flow chamber was disassembled and the surface-capture cells were fixed with 4% paraformaldehyde.

Immunocytochemistry and imaging

The captured cells after fixation were permeabilized with Triton X-100, blocked with 1 wt% BSA in PBS, and stained with anti-wide spectrum cytokeratin (CK), anti-CD45, goat anti-rabbit with Alexa Fluor 647, goat anti-mouse with Alexa Fluor 488, and (4’,6-Diamidino-2-phenylindole) (DAPI) (Myung et al. 2018a). Some samples were additionally

stained with anti-CDX2 and goat anti-rabbit with Alexa Fluor 555. The slides with stained cells were mounted and imaged at 10x magnification with a Zeiss Axio Observer fluorescent microscope equipped with a motorized stage, quadruple bandpass filter, Colibri 7 LED light source and Axiocam 503 camera. Tiled images encompassed the footprint of both flow channels. Colors were balanced manually in Zeiss ZEN software to eliminate excessive background and enhance contrast. Images were exported as single-channel jpegs separated into 16 slices and converted to 8-bit format for image analysis.

Convolutional neural network (CNN) training and validation.

A CNN and a corresponding graphical user interface were developed using Python (v3.0) with Keras (Chollet 2015) and TensorFlow (Abadi et al. 2016). The CNN architecture is included in Supplementary Information (SI). Cells identified as CTCs and several other types of red particles from 10 baseline scans were manually cropped from the exported images and used to train the CNN. True-positive CTCs were confirmed by two trained users. These CTCs consisted of a single, oval blue particle (nucleus) located entirely within a mostly solid-colored red particle (CK) with any overlapping or nearby green signal (CD45) indistinguishable from background or otherwise significantly weaker than nearby leukocytes in a shape that would indicate bleed-through or nonspecific binding.

An automatic thresholding algorithm was applied to each image before particle detection with OpenCV (v3.4.7.28). Each particle in the CK channel centered and cropped down to a 200 × 200 pixel image along with the corresponding DAPI and CD45 channels. A probability was generated for each image with the CNN, then exported along with additional morphological parameters to a separate spreadsheet. Composite images of all suspect CTCs were created and exported for manual validation by a pair of trained users. The process above was programmed into a graphical user interface for routine use. A logistic regression (Logit) model was generated in R (v4.0.3) (Team 2020) incorporating the CNN probability and additional morphological factors and signal intensities derived from all three channels. A probability threshold was determined from the combined CNN and logit model for counting a particle in the CK channel as a CTC.

The validation set consisted of all particles in the CK channel derived from a separate set of 12 slides. Particles were manually classified as true positives by a pair of trained users and compared to the performance of the combined CNN and logit model.

Clinical correlation and statistical analysis

Time points corresponding to chemotherapy and radiation therapy (RT) treatment regimens and clinical outcomes were shared only after collection and quantification of CTC numbers. Patients were evaluated according to RECIST (Response evaluation criteria in solid tumors) (Nishino 2018) by a board-certified radiologist at the University of Iowa. Patients who underwent surgical resection were also assigned pathologic (yp) T and N staging according to the American Joint Commission on Cancer (AJCC) staging criteria 8th edition (Amin et al. 2017). Pathologic complete response (pCR) was defined as the complete absence of viable tumor cells in the primary tumor and regional lymph nodes in the resection specimen. Patients with locally advanced rectal cancer completed post-chemoradiation response

assessment with pelvic MRI and direct tumor visualization using flexible sigmoidoscopy +/− tumor site biopsy (as indicated). Clinical complete response (cCR) was defined as the absence of residual tumor on both endoscopic and MR evaluation. Wilcox signed rank tests were used to CTC counts between subjects with no evidence of disease (NED) at follow-up appointments to those with progression. Kruskal Wallace rank tests were used to compare CTC counts with tumor stage or RECIST outcome. Spearman rank correlation was also used to compare CTC counts across tumor staging criteria.

Results

Identification of CTCs by a machine learning algorithm

A convolutional neural network was developed, trained, and applied to count CK+/CD45− cells from our images. The intrinsic class imbalance (that is, low number of true positives and high number of true negatives) was addressed in two ways. First, only red particles with size and shape approximating a CK-positive cell were considered by the algorithm (Figure 2a). Second, red particles were classified as ‘suspected CTCs’ or one of five separate common false positive types (Figure 2b). The training sets consisted of 1,521 true positive CTCs identified on 10 different pre-treatment samples. Additional 8,252 cells were identified across five classes of false positives, as categorized by CK−/CD45+, CK+/CD45+, CK+/DAPI−, CK low, and debris or artifact. Each cell was subjected to 1000 transformations (mirroring and rotations) to increase the size of the training set.

In order to generate a count of CTCs within a given sample, a binary threshold must be identified to distinguish CTCs from non-CTCs. The CNN output initially produced a highly skewed probability distribution, with many false positives assigned probabilities in excess of 99% (Figure S1a), making threshold selection difficult. Manual validation also revealed a high number of cells with excessive CD45 signal and misshapen nuclei wrongly identified as CTCs. We therefore tested the performance of a second approach – logistic regression – in sorting true positives from false positives using fluorescent signal strength and measures of morphology generated by the particle detection algorithm in OpenCV (including area, circularity, roundness, and solidity) and the relative offset of the centers of the CK particle and DAPI particle. The logit model was fit to a dataset of 600 cells manually classified as true positives or true negatives, resulting in a less-skewed probability distribution when incorporating the CNN probability (Figure S1b) or when run alone (Figure S1c). The CNN, the combined CNN-logit model, and the logit model alone were evaluated using receiver operating characteristics (ROC), which demonstrated a significant benefit to using the combined model (Figure S2). Table S1 lists the parameters driving the combined model, with CNN probability was the single most important parameter driving the logit regression probability ($p < .001$), followed by DAPI circularity ($p < .001$), CD45 signal ($p = .005$), and the relative positioning of the CK and DAPI particles ($p = .034$). Although other morphological parameters and signal strength did not have statistically significant model coefficients, their presence in the model nevertheless improved performance. The threshold for counting a CTC was set to the probability at which the true positive rate plus the false discovery rate equaled 1, resulting in a net count equal to the true count of the 600 cell dataset. This threshold was 0.512 for the combined model (Figure S1e). We next

tested the algorithm with 0.512 threshold on a validation set of 165 true positive CTCs amongst 800,632 particles identified in the CK channel across 12 additional samples. Note that validation set had fewer true positives as a proportion of red particles than the test set. The performance was measured in terms of true positive CTCs amongst all red particles and in terms of CTCs amongst all identified nuclei. By both measures, the algorithm achieved a sensitivity of 0.829 and specificity exceeding 0.999. Accuracy was 0.997 in determining CTCs amongst all red spots and 0.998 in distinguishing CTCs from all cells. The area under the curve (AUC) of the ROC in Figure 2d exceeded 0.998 by both measures, while the precision-recall AUC (AUCPR) was 0.472. An example CTC amongst leukocytes on the capture surface is shown in Figure 2e. Example true positive CTCs are displayed in Figure 2f and non-CTCs with low CNN probability are displayed in Figure 2g.

Enumeration of CTCs in gastrointestinal cancer

The machine learning algorithm described above was used for all clinical CTC enumerations from patient samples. Peripheral blood samples were collected from 27 subjects diagnosed with pancreatic (n = 16), rectal (n = 10), or esophageal (n = 1) adenocarcinoma (Table 1). One subject was dropped from the study after a single time point. Blood samples were drawn at various times during treatment with chemotherapy (22 subjects), radiation therapy (RT) (23 subjects), and surgery (11 subjects). The first samples from 3 patients were discarded due to insufficient separation of a buffy coat layer, and two more failed to arrive for processing within 48 h.

CTCs were detected in samples from all patients. More specifically, four subjects with samples processed prior to chemotherapy had a median of 65.4 CTC ml^{-1} (range 10.0–541.5), all well above the healthy donor median of 0.8 CTC ml^{-1} (Table 2). An additional four pre-treatment subjects had a median 53.0 CTC ml^{-1} (range 0.8–152.3) prior to receiving radiation therapy with one patient right at the healthy donor threshold. Median CTC counts for various time points in treatment are summarized in Table 2. Full results are included in supplementary information (Tables S3 and S4). No statistical relationships were observed between pre-treatment CTC counts and TNM staging criteria or primary tumor site (Table S5), which was consistent with previous results using this technology (Myung et al. 2018b).

Five samples from two subjects were additionally co-stained for CDX2 to provide evidence that enumerated CTCs were characteristic of intestinal epithelial cells. Examples of cells stained with four markers are shown in Figure S3. The proportion of CDX2+ CTCs ranged from a low of 63% to a high of 97% (Figure S4). No cells were observed to express CDX2 without CK. The results strongly suggest a gastrointestinal origin for the detected CTCs.

CTC abundance and response to treatment

CTC abundance and longitudinal trends may reflect treatment success. Figure 3, below, illustrates trends in CTC counts for four subjects over the course of the study. Figure 3a–b shows CTC trends for a pair of patients with no evidence of disease (NED) at their final visit. Samples drawn during chemotherapy or radiation therapy are indicated by horizontal lines. In many subjects with NED, CTC abundance during and following RT was relatively

low compared to pre-therapy counts. In contrast a subject identified as having a partial response (PR) (Figure 3c) following radiation treatment by radiologic RECIST criteria had elevated CTC counts during RT (>10 CTC ml^{-1}). New metastasis was identified shortly after treatment and subsequent CTC counts rose dramatically. In a subject identified as having progressive disease (PD) immediately following RT (Figure 3d), a spike in CTC abundance was detected upon the same follow-up visit.

A majority of recruited subjects underwent neoadjuvant chemotherapy followed by radiation therapy (RT) and surgery (Table S3). The abundance or trends of CTCs during chemotherapy did not appear to correlate well with outcome (Table S4). However, 30 of 33 samples collected during the course of chemotherapy (91%) had counts above 1.0 CTC ml^{-1}. Clinical outcomes were compared to CTC abundance for the 16 subjects receiving RT and having blood draws analyzed immediately before (Pre RT) and during (Mid RT) treatment. Post-treatment (Post RT) counts were collected within 6 months of the end of RT, with a majority of subjects undergoing surgical resection within that time. Subject response to RT was determined by radiologic RECIST criteria as having a complete response (CR) with no NED at follow-up, PR with eventual NED, PR with recurrence, PD. Figure 4a shows no relationship between pre-treatment counts and radiologic outcomes. However, a clear relationship between poorer outcomes and increasing CTC abundance is seen at Mid RT (Figure 4b), within 3 months Post RT (Figure 4c), and between 3 and 6 months Post RT (Figure 4d). Only the 3 month data showed statistically significant differences in CTC counts between subjects with NED and recurrent disease ($p = 0.045$). Pre-treatment counts did not correlate with pathologic staging pre-treatment (rho = −0.042) (Figure 4e). However, a modest trend with post-treatment pathologic staging was seen with Mid RT counts (rho = 0.419) (Figure 4f). A similar relationship was observed when comparing the difference between post- and pre-treatment pathologic staging (rho = 0.389) (Figure 4g), with outliers in each case being subjects that ultimately had NED.

Receiver operating characteristic (ROC) analysis was used to compare the relative performance of Pre, Mid, and Post-treatment CTC abundance with disease recurrence. Results suggest that Mid-RT (area under the curve AUC = 0.73) and 6 month Post-RT (AUC = 0.75) were modestly predictive of the presence of disease following treatment (Figure 4h). Averaging Mid- and Post treatment CTC abundance (Supplemental Figure S5) showed similar performance. In contrast, pre-treatment counts were not predictive (AUC < 0.5).

Discussion

Our highly sensitive CTC detection platform demonstrated unmatched levels of CTC capture in gastrointestinal patients. Significant barriers to routine use of blood tests for gastrointestinal cancer are the low sensitivity and relatively, often resulting in poor correlations with clinical outcome. The reported performance of CellSearch is in line with serum protein biomarkers for pancreatic cancer such as carcinoembryonic antigen (CEA) at 45% sensitivity (Meng et al. 2017), or serum carbohydrate antigen (CA) 19–9 and CA125 at 68% sensitivity (O'Brien et al. 2015). Alternative CTC enumeration technologies in development often report higher detection rates, but relatively low CTC counts. Size-based purification techniques report median of 3 CTCs ml^{-1} or lower in patients with

gastrointestinal cancer (Khoja et al. 2012; Shim et al. 2020; Wu et al. 2015). Antibody-based purification techniques incorporated into microfluidic channels (Rhim et al. 2014; Tsai et al. 2016) are better, with median counts of 2–20 CTCs ml^{-1} for pre-treatment samples depending on tumor stage. The combination of dendrimer-mediated multivalent antibody capture and E-selectin-induced cell rolling reported here produced a median count of over 50 CTCs ml^{-1} in patients before receiving treatment.

The machine learning approach to CTC identification proved to be an efficient and accurate technique to quantify CTC abundance. Many existing technologies, including CellSearch, require human validation of captured CTCs. Human validation is likely to be inconsistent from user-to-user. In our approach and other highly sensitive technologies, human validation may also be unacceptably time consuming. Image analysis algorithms are both faster and more consistent than human users but have difficulty coping with the variability inherent in fluorescent microscopy images of human tissue samples. The limit of relatively straightforward image analysis algorithms was demonstrated by the poor performance of the logit regression model compared to the CNN alone. This work strongly suggests that a machine learning approach is an appropriate middle-ground, achieving greater accuracy than statistical regression with the consistency of a computer algorithm. More importantly, the training set for the CNN may be expanded or replaced for other cancers or tumor markers. The CNN presented here would not detect CTCs expressing specific CK proteins that were not well-stained by the pan-CK antibody, or CTCs that express low levels of CK due to differentiation (Mikolajczyk et al. 2011; Serrano et al. 2014). Immunocytochemical detection of other tumor markers and subsequent CNN re-training may further enhance the sensitivity of this approach. The approach reported here was also optimized for isolated CTCs and may not accurately identify cell clusters, which may have a higher propensity to metastasize than individual CTCs (Giuliano et al. 2018). Such clusters are rarely observed on our biomimetic surfaces. They may break apart during rolling or otherwise avoid capture due to higher shear stresses than single cells.

Longitudinal trends of CTC abundance likely reflect treatment success, as we previously published primarily based on an HNSCC cohort receiving radiotherapy (Myung et al. 2018b). The results strongly suggest that CTC abundance during and immediately following preoperative chemoradiation may predict outcome. However, some patients with confirmed recurrent disease had CTC levels below healthy donor controls. A moderate correlation was observed between mid-RT CTC counts and RECIST outcome. Consistent with our previous work, we observed a decrease in median CTC counts during and after RT. Three of 4 patients with CR, and 5 of 7 patients with eventual NED had a net decrease in CTC abundance when comparing pre- vs. post-RT counts. However, in this cohort, we observed a stronger correlation of outcome with mid-RT CTC count than with longitudinal trends. The identification of accurate biomarkers is particularly relevant to GI cancers. There is growing prospective evidence that patients with locally advanced rectal cancer who achieve complete responses to neoadjuvant chemotherapy and radiation may be eligible for non-surgical management though uncertainties in accurately identifying complete responses and detecting early recurrences has limited its broader adoption. In pancreatic cancer, recurrence progression is extremely common and can be very difficult to assess radiographically after a Whipple resection in the setting of profound post-surgical changes. High CTC counts

during treatment may inform adjuvant treatment decisions. Alternatively, CTC abundance may help surgeons avoid a non-curative surgery after neoadjuvant therapy in patients with occult metastatic disease.

The wide diversity of treatment regimens made drawing further conclusions difficult. For instance, six pancreatic cancer patients received chemotherapy without any RT or surgery. All patients had detectable CTCs at levels higher than the healthy donor threshold for each sample collected during and following treatment (Table S4). However, consistent trends were not discernable, and all chemotherapy-only patients were reported as having residual or progressive disease following treatment. Although the abundance of CTCs during chemotherapy treatments may not have predictive value, they are present in high numbers. Further analysis of protein expression or transcription patterns may prove to be more predictive than abundance alone.

Conclusion

The effective treatment of gastrointestinal cancer is hindered by a lack of clinically relevant biomarkers. The enumeration of CTCs from peripheral blood samples has shown promise, but widespread clinical adoption will require new technologies capable of isolating the rare cells at high sensitivity and accuracy in enumeration. In this work, a highly sensitive CTC purification platform based on biomimetic cell rolling and dendrimer-mediated multivalent binding captured significantly more CTC than other published reports with gastrointestinal cancer. A machine learning approach was developed, validated, and deployed to efficiently count the large number of captured CTCs. The results suggested that CTC abundance during and immediately following treatment have potential as a predictive biomarker as we found that changes in CTCs during radiation therapy correlated with clinical outcome in most patients.

Supplementary Material

Refer to Web version on PubMed Central for supplementary material.

Acknowledgements

This study was partially supported by the Wisconsin Head and Neck cancer SPORE grant funded by the National Institute of Health (NIH) [grant number P50CA278595], National Cancer Institute (NCI) SBIR [grant number 1R43CA232924], the UW Office of the Vice Chancellor for Research and Graduate Education State Economic Engagement and Development (OVCGRE SEED) Program, and the Milton J. Henrichs Chair Fund. The authors would like to thank Jennifer Larson for her support in arranging patient sample collection and shipment. Dr. Sin-Jung Park and Dr. Woo-jin Jeong, DaWon Kim, and Brigita Meskauskaite contributed to sample processing. Dr. KiChang Nam provided valuable advice for machine learning development and validation.

Glossary

MJP	Methodology, Formal Analsis, Investigation, Writing – Original Draft.
JB	Investigation, Formal Analysis
SL	Software

AZW	Conceptualization, Supervision
SNN	Resources
CC	Resources, Supervision
HH	Conceptualization
JMC	Conceptualization, Resources
YSK	Conceptualization
SH	Conceptualization, Methodology, Writing – Original Draft, Supervision, Project Administration, Funding Acquisition

References

Abadi M, Agarwal A, Barham P, Brevdo E, Chen Z, Citro C, Corrado GS, Davis A, Dean J, Devin M, 2016. Tensorflow: Large-scale machine learning on heterogeneous distributed systems. arXiv preprint arXiv:1603.04467

ACS, 2022. Cancer Facts & Figures 2022. American Cancer Society, Atlanta, GA.

Albawi S, Mohammed TA, Al-Zawi S, 2017. Understanding of a convolutional neural network. 2017 International Conference on Engineering and Technology (ICET), pp. 1–6.

Amin MB, Greene FL, Edge SB, Compton CC, Gershenwald JE, Brookland RK, Meyer L, Gress DM, Byrd DR, Winchester DP, 2017. The Eighth Edition AJCC Cancer Staging Manual: Continuing to build a bridge from a population-based to a more “personalized” approach to cancer staging. CA: A Cancer Journal for Clinicians 67(2), 93–99. [PubMed: 28094848]

Bidard FC, Huguet F, Louvet C, Mineur L, Bouché O, Chibaudel B, Artru P, Desseigne F, Bachet JB, Mathiot C, Pierga JY, Hammel P, 2013. Circulating tumor cells in locally advanced pancreatic adenocarcinoma: the ancillary CirCe 07 study to the LAP 07 trial. Annals of oncology : official journal of the European Society for Medical Oncology 24(8), 2057–2061. [PubMed: 23676420]

Bu J, Nair A, Iida M, Jeong WJ, Poellmann MJ, Mudd K, Kubiatowicz LJ, Liu EW, Wheeler DL, Hong S, 2020a. An Avidity-Based PD-L1 Antagonist Using Nanoparticle-Antibody Conjugates for Enhanced Immunotherapy. Nano letters 20(7), 4901–4909. [PubMed: 32510959]

Bu J, Nair A, Kubiatowicz LJ, Poellmann MJ, Jeong W. j., Reyes-Martinez M, Armstrong AJ, George DJ, Wang AZ, Zhang T, Hong S, 2020b. Surface engineering for efficient capture of circulating tumor cells in renal cell carcinoma: From nanoscale analysis to clinical application. Biosensors and Bioelectronics 162, 112250. [PubMed: 32392161]

Bu J, Nair A, Kubiatowicz LJ, Poellmann MJ, Jeong WJ, Reyes-Martinez M, Armstrong AJ, George DJ, Wang AZ, Zhang T, Hong S, 2020c. Surface engineering for efficient capture of circulating tumor cells in renal cell carcinoma: From nanoscale analysis to clinical application. Biosensors & bioelectronics 162, 112250. [PubMed: 32392161]

Cayrefourcq L, Mazard T, Joosse S, Solassol J, Ramos J, Assenat E, Schumacher U, Costes V, Maudelonde T, Pantel K, Alix-Panabières C, 2015. Establishment and Characterization of a Cell Line from Human Circulating Colon Cancer Cells. Cancer research 75(5), 892. [PubMed: 25592149]

Chollet F, 2015. keras

Cohen SJ, Punt CJ, Iannotti N, Saidman BH, Sabbath KD, Gabrail NY, Picus J, Morse M, Mitchell E, Miller MC, Doyle GV, Tissing H, Terstappen LW, Meropol NJ, 2008. Relationship of circulating tumor cells to tumor response, progression-free survival, and overall survival in patients with metastatic colorectal cancer. Journal of clinical oncology : official journal of the American Society of Clinical Oncology 26(19), 3213–3221. [PubMed: 18591556]

Dotan E, Alpaugh RK, Ruth K, Negin BP, Denlinger CS, Hall MJ, Astsaturov I, McAleer C, Fittipaldi P, Thrash-Bingham C, Meropol NJ, Cohen SJ, 2016. Prognostic Significance of MUC-1 in

Circulating Tumor Cells in Patients With Metastatic Pancreatic Adenocarcinoma. Pancreas 45(8), 1131–1135. [PubMed: 26967453]

Erickson BJ, Korfiatis P, Akkus Z, Kline TL, 2017. Machine Learning for Medical Imaging. Radiographics : a review publication of the Radiological Society of North America, Inc 37(2), 505–515. [PubMed: 28212054]

Giuliano M, Shaikh A, Lo HC, Arpino G, De Placido S, Zhang XH, Cristofanilli M, Schiff R, Trivedi MV, 2018. Perspective on Circulating Tumor Cell Clusters: Why It Takes a Village to Metastasize. Cancer research 78(4), 845–852. [PubMed: 29437766]

Gorges TM, Stein A, Quidde J, Hauch S, Röck K, Riethdorf S, Joosse SA, Pantel K, 2016. Improved Detection of Circulating Tumor Cells in Metastatic Colorectal Cancer by the Combination of the CellSearch® System and the AdnaTest®. PLOS ONE 11(5), e0155126. [PubMed: 27182774]

He B, Lu Q, Lang J, Yu H, Peng C, Bing P, Li S, Zhou Q, Liang Y, Tian G, 2020. A New Method for CTC Images Recognition Based on Machine Learning. Frontiers in Bioengineering and Biotechnology 8(897).

Heitzer E, Auer M, Gasch C, Pichler M, Ulz P, Hoffmann EM, Lax S, Waldispuehl-Geigl J, Mauermann O, Lackner C, Höfler G, Eisner F, Sill H, Samonigg H, Pantel K, Riethdorf S, Bauernhofer T, Geigl JB, Speicher MR, 2013. Complex tumor genomes inferred from single circulating tumor cells by array-CGH and next-generation sequencing. Cancer research 73(10), 2965–2975. [PubMed: 23471846]

Hiraiwa K, Takeuchi H, Hasegawa H, Saikawa Y, Suda K, Ando T, Kumagai K, Irino T, Yoshikawa T, Matsuda S, Kitajima M, Kitagawa Y, 2008. Clinical Significance of Circulating Tumor Cells in Blood from Patients with Gastrointestinal Cancers. Annals of Surgical Oncology 15(11), 3092. [PubMed: 18766405]

Hong S, Lee D, Zhang H, Zhang JQ, Resvick JN, Khademhosseini A, King MR, Langer R, Karp JM, 2007. Covalent immobilization of p-selectin enhances cell rolling. Langmuir : the ACS journal of surfaces and colloids 23(24), 12261–12268. [PubMed: 17949112]

Iwatsuki M, Toyoshima K, Watanabe M, Hayashi N, Ishimoto T, Eto K, Iwagami S, Baba Y, Yoshida N, Hayashi A, Ohta Y, Baba H, 2013. Frequency of HER2 expression of circulating tumour cells in patients with metastatic or recurrent gastrointestinal cancer. British Journal of Cancer 109(11), 2829–2832. [PubMed: 24201755]

Jin S-E, Bae JW, Hong S, 2010. Multiscale observation of biological interactions of nanocarriers: From nano to macro. Microscopy Research and Technique 73(9), 813–823. [PubMed: 20232368]

Khoja L, Backen A, Sloane R, Menasce L, Ryder D, Krebs M, Board R, Clack G, Hughes A, Blackhall F, Valle JW, Dive C, 2012. A pilot study to explore circulating tumour cells in pancreatic cancer as a novel biomarker. Br J Cancer 106(3), 508–516. [PubMed: 22187035]

Lannin TB, Thege FI, Kirby BJ, 2016. Comparison and optimization of machine learning methods for automated classification of circulating tumor cells. Cytometry Part A 89(10), 922–931.

Lee JS, Park SS, Lee YK, Norton JA, Jeffrey SS, 2019. Liquid biopsy in pancreatic ductal adenocarcinoma: current status of circulating tumor cells and circulating tumor DNA. Molecular oncology 13(8), 1623–1650. [PubMed: 31243883]

Madabhushi A, Lee G, 2016. Image analysis and machine learning in digital pathology: Challenges and opportunities. Medical Image Analysis 33, 170–175. [PubMed: 27423409]

McEver RP, Zhu C, 2010. Rolling cell adhesion. Annual review of cell and developmental biology 26, 363–396.

Meng Q, Shi S, Liang C, Liang D, Xu W, Ji S, Zhang B, Ni Q, Xu J, Yu X, 2017. Diagnostic and prognostic value of carcinoembryonic antigen in pancreatic cancer: a systematic review and meta-analysis. OncoTargets and therapy 10, 4591–4598. [PubMed: 28979147]

Mikolajczyk SD, Millar LS, Tsinberg P, Coutts SM, Zomorrodi M, Pham T, Bischoff FZ, Pircher TJ, 2011. Detection of EpCAM-Negative and Cytokeratin-Negative Circulating Tumor Cells in Peripheral Blood. Journal of oncology 2011, 252361. [PubMed: 21577258]

Myung JH, Cha A, Tam KA, Poellmann M, Borgeat A, Sharifi R, Molokie RE, Votta-Velis G, Hong S, 2019. Dendrimer-Based Platform for Effective Capture of Tumor Cells after TGFβ1-Induced Epithelial–Mesenchymal Transition. Analytical Chemistry 91(13), 8374–8382. [PubMed: 31247718]

Myung JH, Eblan MJ, Caster JM, Park S-J, Poellmann MJ, Wang K, Tam KA, Miller SM, Shen C, Chen RC, Zhang T, Tepper JE, Chera BS, Wang AZ, Hong S, 2018a. Multivalent Binding and Biomimetic Cell Rolling Improves the Sensitivity and Specificity of Circulating Tumor Cell Capture. Clinical Cancer Research 24(11), 2539–2547. [PubMed: 29545463]

Myung JH, Eblan MJ, Caster JM, Park SJ, Poellmann MJ, Wang K, Tam KA, Miller SM, Shen C, Chen RC, Zhang T, Tepper JE, Chera BS, Wang AZ, Hong S, 2018b. Multivalent Binding and Biomimetic Cell Rolling Improves the Sensitivity and Specificity of Circulating Tumor Cell Capture. Clinical cancer research : an official journal of the American Association for Cancer Research 24(11), 2539–2547. [PubMed: 29545463]

Myung JH, Gajjar KA, Chen J, Molokie RE, Hong S, 2014a. Differential Detection of Tumor Cells Using a Combination of Cell Rolling, Multivalent Binding, and Multiple Antibodies. Analytical chemistry.

Myung JH, Gajjar KA, Chen J, Molokie RE, Hong S, 2014b. Differential Detection of Tumor Cells Using a Combination of Cell Rolling, Multivalent Binding, and Multiple Antibodies. Analytical Chemistry 86(12), 6088–6094. [PubMed: 24892731]

Myung JH, Gajjar KA, Saric J, Eddington DT, Hong S, 2011a. Dendrimer-mediated multivalent binding for the enhanced capture of tumor cells. Angewandte Chemie (International ed. in English) 50(49), 11769–11772. [PubMed: 22012872]

Myung JH, Gajjar KA, Saric J, Eddington DT, Hong S, 2011b. Dendrimer-Mediated Multivalent Binding for the Enhanced Capture of Tumor Cells. Angewandte Chemie International Edition 50(49), 11769–11772. [PubMed: 22012872]

Myung JH, Launiere CA, Eddington DT, Hong S, 2010. Enhanced tumor cell isolation by a biomimetic combination of E-selectin and anti-EpCAM: implications for the effective separation of circulating tumor cells (CTCs). Langmuir : the ACS journal of surfaces and colloids 26(11), 8589–8596. [PubMed: 20155985]

Myung JH, Park SJ, Wang AZ, Hong S, 2018c. Integration of biomimicry and nanotechnology for significantly improved detection of circulating tumor cells (CTCs). Advanced drug delivery reviews 125, 36–47. [PubMed: 29247765]

Myung JH, Roengvoraphoj M, Tam KA, Ma T, Memoli VA, Dmitrovsky E, Freemantle SJ, Hong S, 2015. Effective Capture of Circulating Tumor Cells from a Transgenic Mouse Lung Cancer Model Using Dendrimer Surfaces Immobilized with Anti-EGFR. Analytical chemistry 87(19), 10096–10102. [PubMed: 26312815]

Nakamichi K, Lu H, Kim H, Yoneda K, Tanaka F, 2019. Classification of Circulating Tumor Cells in Fluorescence Microscopy Images Based on SqueezeNet. 2019 19th International Conference on Control, Automation and Systems (ICCAS), pp. 1042–1045.

Nishino M, 2018. Tumor Response Assessment for Precision Cancer Therapy: Response Evaluation Criteria in Solid Tumors and Beyond. American Society of Clinical Oncology Educational Book(38), 1019–1029. [PubMed: 30231378]

Normanno N, Cervantes A, Ciardiello F, De Luca A, Pinto C, 2018. The liquid biopsy in the management of colorectal cancer patients: Current applications and future scenarios. Cancer Treatment Reviews 70, 1–8. [PubMed: 30053724]

O'Brien DP, Sandanayake NS, Jenkinson C, Gentry-Maharaj A, Apostolidou S, Fourkala EO, Camuzeaux S, Blyuss O, Gunu R, Dawnay A, Zaikin A, Smith RC, Jacobs IJ, Menon U, Costello E, Pereira SP, Timms JF, 2015. Serum CA19–9 is significantly upregulated up to 2 years before diagnosis with pancreatic cancer: implications for early disease detection. Clinical cancer research : an official journal of the American Association for Cancer Research 21(3), 622–631. [PubMed: 24938522]

Okubo K, Uenosono Y, Arigami T, Mataki Y, Matsushita D, Yanagita S, Kurahara H, Sakoda M, Kijima Y, Maemura K, Natsugoe S, 2017. Clinical impact of circulating tumor cells and therapy response in pancreatic cancer. European journal of surgical oncology : the journal of the European Society of Surgical Oncology and the British Association of Surgical Oncology 43(6), 1050–1055. [PubMed: 28233633]

Palta M, Godfrey D, Goodman KA, Hoffe S, Dawson LA, Dessert D, Hall WA, Herman JM, Khorana AA, Merchant N, Parekh A, Patton C, Pepek JM, Salama JK, Tuli R, Koong AC, 2019. Radiation

Therapy for Pancreatic Cancer: Executive Summary of an ASTRO Clinical Practice Guideline. Practical radiation oncology 9(5), 322–332. [PubMed: 31474330]

Pernot S, Badoual C, Terme M, Castan F, Cazes A, Bouche O, Bennouna J, Francois E, Ghiringhelli F, De La Fouchardiere C, Samalin E, Bachet JB, Borg C, Ducreux M, Marcheteau E, Stanbury T, Gourgou S, Malka D, Taieb J, 2017. Dynamic evaluation of circulating tumour cells in patients with advanced gastric and oesogastric junction adenocarcinoma: Prognostic value and early assessment of therapeutic effects. European Journal of Cancer 79, 15–22. [PubMed: 28456090]

Poellmann MJ, Nair A, Bu J, Kim JKH, Kimple RJ, Hong S, 2020. Immunoavidity-Based Capture of Tumor Exosomes Using Poly(amidoamine) Dendrimer Surfaces. Nano letters 20(8), 5686–5692. [PubMed: 32407121]

Poellmann MJ, Rawding P, Kim D, Bu J, Kim Y, Hong S, 2022. Branched, dendritic, and hyperbranched polymers in liquid biopsy device design. Wiley interdisciplinary reviews. Nanomedicine and nanobiotechnology 14(3), e1770. [PubMed: 34984833]

Rhim AD, Thege FI, Santana SM, Lannin TB, Saha TN, Tsai S, Maggs LR, Kochman ML, Ginsberg GG, Lieb JG, Chandrasekhara V, Drebin JA, Ahmad N, Yang YX, Kirby BJ, Stanger BZ, 2014. Detection of circulating pancreas epithelial cells in patients with pancreatic cystic lesions. Gastroenterology 146(3), 647–651. [PubMed: 24333829]

Riethdorf S, O'Flaherty L, Hille C, Pantel K, 2018. Clinical applications of the CellSearch platform in cancer patients. Advanced drug delivery reviews 125, 102–121. [PubMed: 29355669]

Serrano MJ, Ortega FG, Alvarez-Cubero MJ, Nadal R, Sanchez-Rovira P, Salido M, Rodríguez M, García-Puche JL, Delgado-Rodriguez M, Solé F, García MA, Perán M, Rosell R, Marchal JA, Lorente JA, 2014. EMT and EGFR in CTCs cytokeratin negative non-metastatic breast cancer. Oncotarget 5(17).

Shim JE, Bu J, Lee MK, Cho YH, Kim TH, Bu JU, Han SW, 2020. Viable and high-throughput isolation of heterogeneous circulating tumor cells using tapered-slit filters. Sens. Actuator B-Chem 321, 8.

Sunoqrot S, Liu Y, Kim D-H, Hong S, 2013. In Vitro Evaluation of Dendrimer–Polymer Hybrid Nanoparticles on Their Controlled Cellular Targeting Kinetics. Molecular Pharmaceutics 10(6), 2157–2166. [PubMed: 23234605]

Team RC, 2020. R: A language and environment for statistical computing. 4.0.3 ed. R Foundation for Statistical Computing, Vienna, Austria.

Tsai W-S, Chen J-S, Shao H-J, Wu J-C, Lai J-M, Lu S-H, Hung T-F, Chiu Y-C, You J-F, Hsieh P-S, Yeh C-Y, Hung H-Y, Chiang S-F, Lin G-P, Tang R, Chang Y-C, 2016. Circulating Tumor Cell Count Correlates with Colorectal Neoplasm Progression and Is a Prognostic Marker for Distant Metastasis in Non-Metastatic Patients. Scientific Reports 6(1), 24517. [PubMed: 27075165]

van Dalum G, Stam G-J, Scholten LFA, Mastboom WJB, Vermes I, Tibbe AGJ, De Groot MR, Terstappen LWMM, 2015. Importance of circulating tumor cells in newly diagnosed colorectal cancer. Int J Oncol 46(3), 1361–1368. [PubMed: 25572133]

Wang P-X, Sun Y-F, Jin W-X, Cheng J-W, Peng H-X, Xu Y, Zhou K-Q, Chen L-M, Huang K, Wu S-Y, Hu B, Zhang Z-F, Guo W, Cao Y, Zhou J, Fan J, Yang X-R, 2021. Circulating tumor cell detection and single-cell analysis using an integrated workflow based on ChimeraX®-i120 Platform: A prospective study. Molecular Oncology 15(9), 2345–2362. [PubMed: 33301640]

Wo JY, Anker CJ, Ashman JB, Bhadkamkar NA, Bradfield L, Chang DT, Dorth J, Garcia-Aguilar J, Goff D, Jacqmin D, Kelly P, Newman NB, Olsen J, Raldow AC, Ruiz-Garcia E, Stitzenberg KB, Thomas CR Jr., Wu QJ, Das P, 2021. Radiation Therapy for Rectal Cancer: Executive Summary of an ASTRO Clinical Practice Guideline. Practical radiation oncology 11(1), 13–25. [PubMed: 33097436]

Wu S, Liu S, Liu Z, Huang J, Pu X, Li J, Yang D, Deng H, Yang N, Xu J, 2015. Classification of Circulating Tumor Cells by Epithelial-Mesenchymal Transition Markers. PLOS ONE 10(4), e0123976. [PubMed: 25909322]

Highlights:

- Nanostructured, biomimetic liquid biopsy captured high numbers of GI cancer CTCs
- Machine learning algorithm efficiently enumerated immunocytochemically labeled CTCs
- CTC abundance immediately following treatment predicted disease recurrence

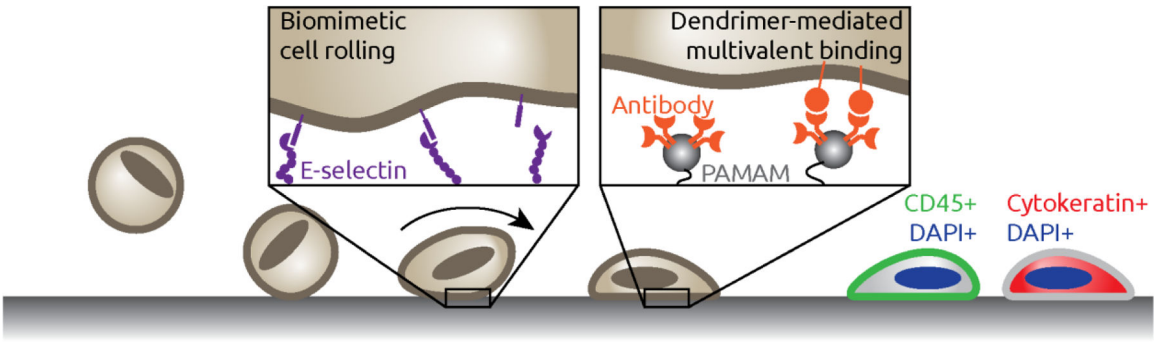

Figure 1.

Purification of circulating tumor cells from peripheral blood mononuclear cells in a flow chamber by biomimetic cell rolling on E-selectin and dendrimer-mediated multivalent binding. The CTCs are distinguished from nonspecifically-captured cells by immunocytochemistry.

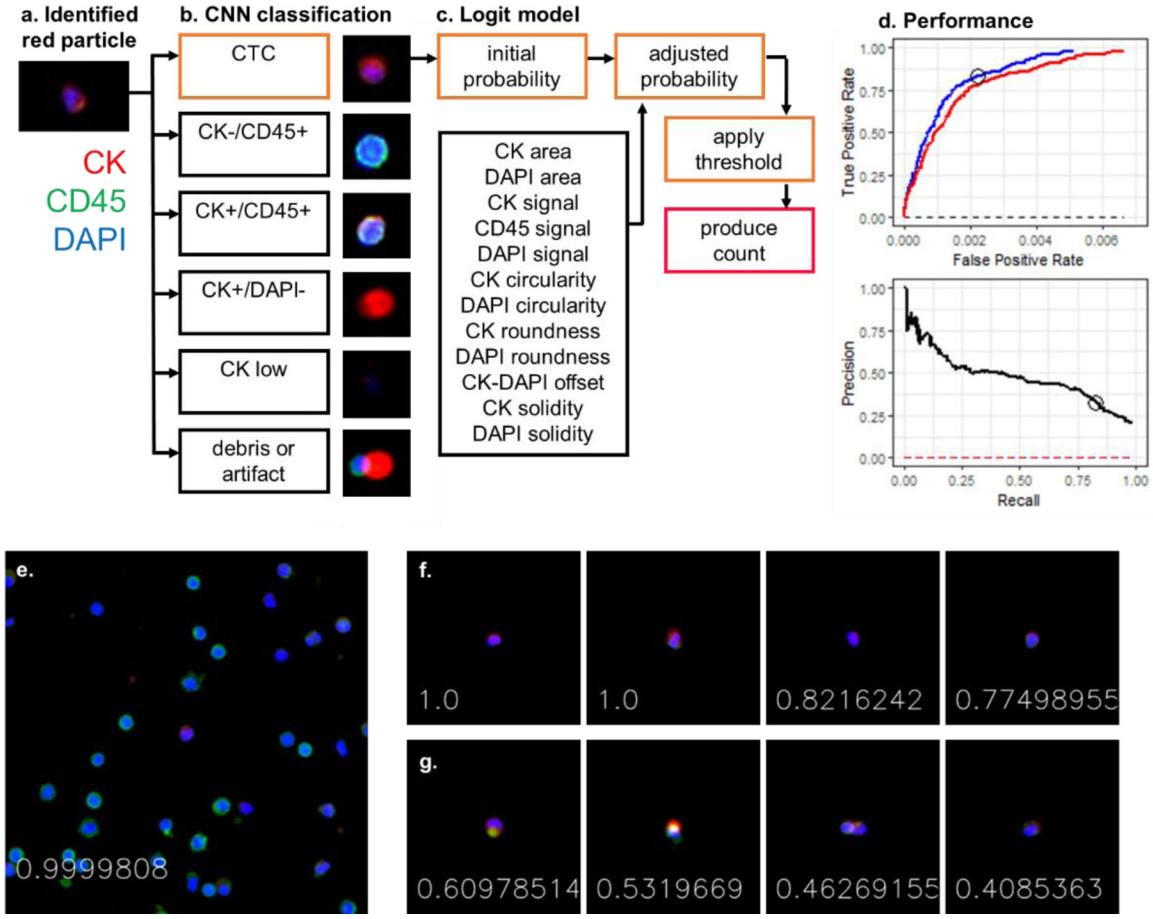

Figure 2.

Machine learning for CTC enumeration. a) Particles containing CK signal (red) were identified from scans of clinical samples, cropped, and cleaned. b) The CNN categorized the particle as a likely CTC or one of five false positives. c) The CNN probability was adjusted by logit regression to increase accuracy. d) ROC and precision-recall analysis of the machine learning algorithm. Blue line represents performance in terms of nuclei, red line represents performance in terms of spots in the CK (red) channel, dashed lines indicate 'no skill' performance, and circle illustrates threshold used in clinical sample analysis. e) An example of a positively-identified CTC (red) on the capture surface amongst leukocytes (green). The number indicates the CNN probability. f) Examples of true positive CTCs. g) Examples of red particles with CNN probability too low to be counted as CTCs.

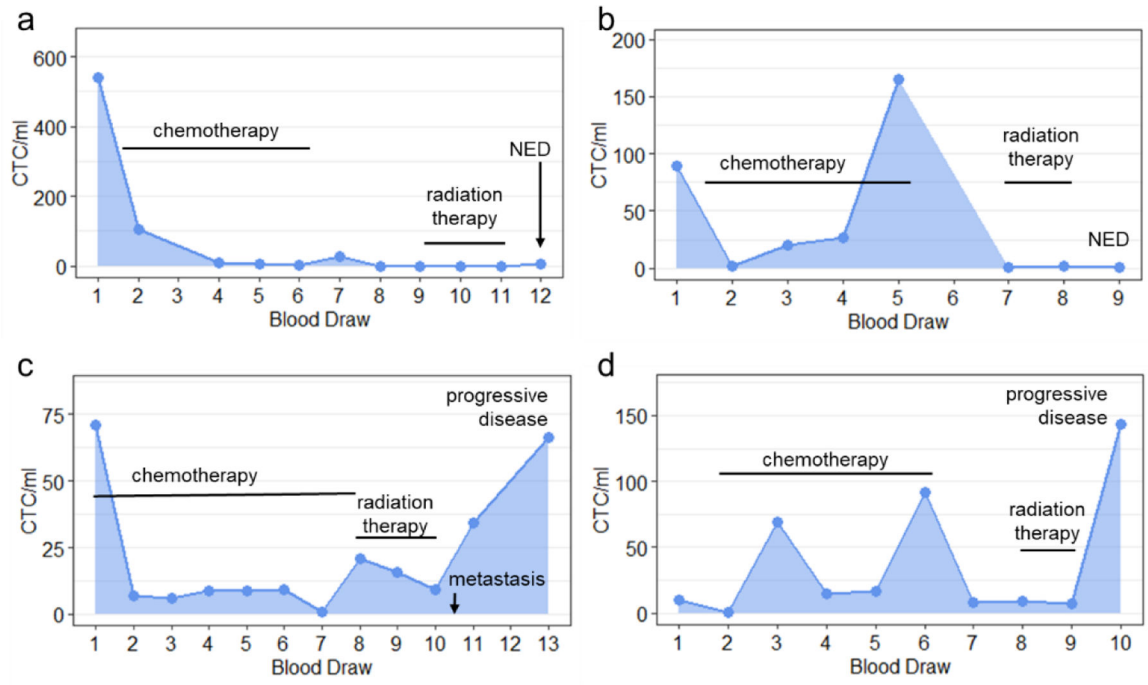

Figure 3.

Select CTC trends annotated with treatments and clinical observations for subjects (a) 08, (b) 10, (c) 13, and (d) 15.

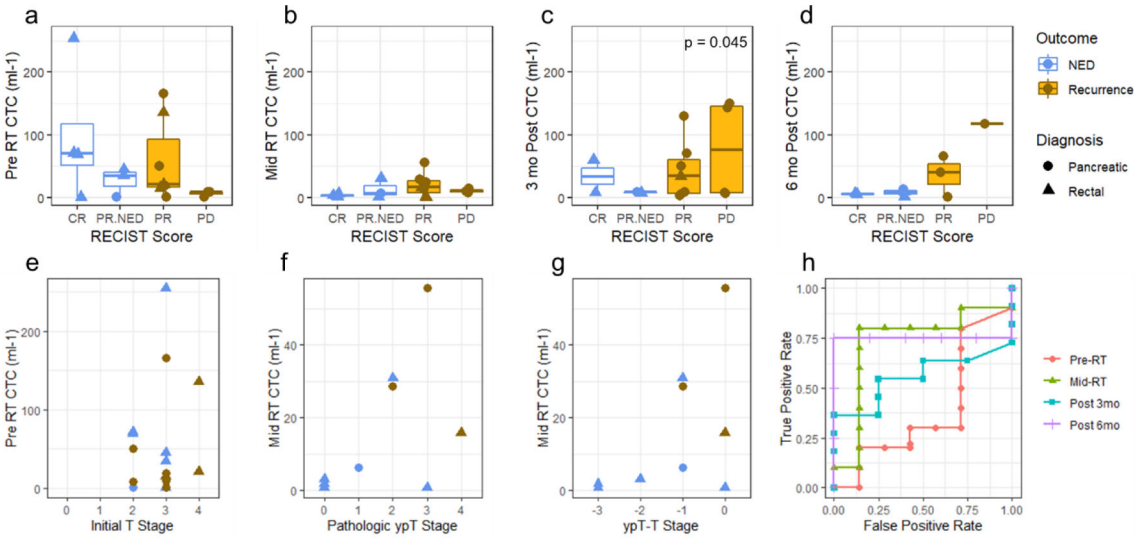

Figure 4.

CTC abundance compared to radiological response to treatment a) prior to RT, b) during RT, c) within 3 months of completing RT, and d) within 6 months of completing RT. e) Pre-treatment counts did not correlate with pathologic staging prior to treatment. CTC abundance during RT did trend with f) pathologic staging of tumors post-treatment and g) the difference between post- and pre-treatment staging. h) ROC analysis of CTC abundance and disease recurrence. AUC for Pre-, Mid-, 3 month Post-, and 6 month Post-RT were 0.39, 0.73, 0.57, and 0.75.

Table 1.

Demographic characteristics and tumor staging of subjects prior to treatment

Age	range 44–80
	mean 62
	median 64
Sex	17 male
	10 female
Race	26 white
	1 multi-racial
Tumor site	16 pancreatic adenocarcinoma
	10 rectal adenocarcinoma
	1 esophageal adenocarcinoma
T score	0 T1
	7 T2
	14 T3
	6 T4
N score	10 N0
	10 N1
	7 N2
M score	15 M0
	11 M1

Table 2.

CTC counts grouped by treatment stage

Time Point	n	Median	Minimum	Maximum
Pre-Chemotherapy	4	65.4	10.0	541.5
Pre-RT without Chemo	4	53.0	0.8	152.3
Post-Chemo, Pre-RT	14	19.6	0.4	254.5
Mid-RT	17	7.4	0.2	55.5
Post-RT, prior to surgery	11	2.3	0.2	244.6
0–3 months post-treatment	15	9.1	3.1	150.0
3–6 months post-treatment	9	8.7	0.5	118.0